論文 / 著書情報
Article / Book Information

Title	Effect of rafted microstructure and its temperature dependency on fatigue crack propagation in a single-crystal Ni-base superalloy
Authors	Motoki Sakaguchi, Ryota Okamoto, Takanori Karato, Kenta Suzuki
Citation	Fatigue & Fracture of Engineering Materials & Structures, Vol. 46, No. 2, pp. 590-602
Pub. date	2023, 2
DOI	https://doi.org/10.1111/ffe.13888
Creative Commons	Information is in the article.

Received: 25 February 2022 | Revised: 13 October 2022 | Accepted: 23 October 2022

DOI: 10.1111/ffe.13888

ORIGINAL ARTICLE

FFEMS Fatigue & Fracture of Engineering Materials & Structures

WILEY

Effect of rafted microstructure and its temperature dependency on fatigue crack propagation in a single-crystal Ni-base superalloy

Motoki Sakaguchi[1] | **Ryota Okamoto**[1] | **Takanori Karato**[2] | **Kenta Suzuki**[2]

[1]Department of Mechanical Engineering, Tokyo Institute of Technology, Tokyo, Japan

[2]Mitsubishi Heavy Industries, Ltd., Takasago-shi, Hyogo, Japan

Correspondence
Motoki Sakaguchi, Department of Mechanical Engineering, Tokyo Institute of Technology, O-okayama 2-12-1, Meguro-ku, Tokyo 152-8552, Japan.
Email: sakaguchi.m.ac@m.titech.ac.jp

Abstract

Effects of rafted microstructure and its temperature dependency on fatigue crack propagation (FCP) in a single-crystal Ni-base superalloy are experimentally investigated. FCP tests are conducted at room temperature, 450°C, and 700°C for two types of pre-rafted specimens, and their FCP behaviors are compared with that of a specimen with cuboidal γ′ precipitates. It is found in the experiments that there is no significant influence of rafted microstructures on FCP rate at room temperature, while a clear influence is pronounced at 450 and 700°C depending on the coarsening direction of rafted microstructures and the level of stress intensity factor range. The temperature dependency in the effect of rafted microstructure is discussed with special considerations on the microscopic FCP behavior affected by the morphology of γ′ precipitates, the coherency of the γ/γ′ interface, and temperature-dependent slip characteristics of γ and γ′ phases.

KEYWORDS

fatigue crack propagation, Ni-base superalloy, rafting, temperature dependency, γ/γ′ microstructure

1 | INTRODUCTION

Single-crystal Ni-base superalloys have been widely used for high-temperature components in gas turbine and jet engine applications, since they have superior high-temperature strength as well as excellent corrosion and oxidation resistance. Generally, the superalloys have a composite microstructure consisting of cuboidal γ′ precipitates surrounded by narrow channels of the γ matrix. Extensive studies have suggested that the superior mechanical properties of single-crystal superalloys are associated with the unique characteristics of the γ/γ′ microstructure, including an internal stress field induced by the lattice misfit of the coherent γ/γ′ interface and the strength of γ′ precipitates that increases with temperature.[1–5]

High-temperature components of a gas turbine system experience severe thermal stress due to repeated start-up and shut-down cycles in addition to centrifugal forces at elevated temperature. Many studies have investigated to predict the remaining life of superalloy components based on fracture mechanics focusing on fatigue crack propagation (FCP) behavior in single-crystal Ni-base superalloys.[2,3,6–19] In particular, a lot of attention has been paid to the effects of temperature,[6–10,13] loading condition,[6,9,10,15,16] and crystal orientation[8,9,11–14,17] on

FCP behavior. In these studies, the unique characteristics of the γ/γ′ microstructure also play an important role that determines the microscopic and macroscopic FCP behaviors. The role of γ′ precipitates in FCP has been first addressed by Telesman et al.,[18] who investigated FCP behaviors in a single-crystal Ni-base superalloy, PWA1480, at room temperature (RT). They revealed that the γ′ precipitate plays a barrier role to dislocation motion and affects the macroscopic FCP mode depending on the level of stress intensity factor range, ΔK. Sengupta et al.[2] prepared two types of single-crystal specimens with different sizes of γ′ precipitates by applying different heat treatments and conducted FCP tests at RT. They found that a smaller γ′ precipitate leads to a higher fatigue threshold and lower FCP rate in the near-threshold region. They also conducted similar FCP tests at 650°C[3] and reported that the results are opposite to those at RT: That is, a larger γ′ precipitate causes a higher fatigue threshold and lower FCP rate at 650°C. Suzuki et al.[19] conducted FCP tests at RT, 450°C, and 700°C using four types of compact (C(T)) specimens with different combinations of crystal orientations in loading and crack propagation directions. They revealed that the fatigue crack propagates in the crystallographic shearing mode at RT, while the crack transitions its propagation mode from the opening to the shearing mode at 450 and 700°C. They suggested that such a temperature-dependent FCP behavior is attributed to the changes of microscopic deformation depending on the distinctive temperature dependency of the γ′ precipitate. Although these studies have demonstrated that the γ/γ′ microstructure plays some important roles in FCP behavior, several issues have not been fully clarified yet, particularly regarding the effects of the γ′ morphology, coherent γ/γ′ interface, and temperature-dependent slip characteristics of γ and γ′ phases. A rafting phenomenon, which is a unique microstructural evolution in Ni-base superalloys, is suitable to examine these effects of the γ/γ′ microstructure.

The rafting phenomenon is a microstructural change accompanied by severe directional coarsening of the initially cuboidal γ′ precipitates to plate-like (normal to the stress axis) or needle-like (parallel to the stress axis) structure induced by creep stress.[20–24] The direction and the extent of coarsening are determined by the sign and the magnitude of the γ/γ′ lattice misfit and those of the externally applied stress.[20] It has been proven that the fundamental process of the rafting is associated with the locally inhomogeneous creep deformation and the subsequent reaction of piled-up dislocation at the γ/γ′ interface, which leads to an inhomogeneous misfit relaxation and a potential energy gradient. Several studies have investigated influences of rafted microstructures on high-temperature fatigue properties.[8,25–28] Ott and Mughrabi[25] conducted low cycle fatigue (LCF) tests at 950 and 1050°C for CMSX-4 specimens with three different microstructures: initial γ/γ′ with cuboidal γ′, plate-like rafted, and needle-like rafted microstructures. They showed that the LCF life of the plate-like rafted microstructure is reduced, while that of the needle-like microstructure is extended. Sakaguchi and Okazaki[26] proposed an extended micromechanics model based on Eshelby's equivalent inclusion theory and numerically indicated that the plate-type rafted microstructure has a detrimental effect on the high-temperature LCF strength for negative misfit superalloys. Epishin et al.[27] performed the LCF tests at 750 and 950°C for the plate-type rafted specimens and revealed that the rafted microstructure leads to a remarkable reduction of LCF life, particularly under a smaller strain amplitude at 750°C. Most recently, Yang et al.[28] performed a stress-controlled LCF test at 980°C for central-hole specimens with an inhomogeneous rafted microstructure and indicated that pre-rafting treatment significantly decreases the LCF life relating to a degradation of the resistance to plastic deformation. These studies have focused on the total fatigue lives under LCF loading at higher temperatures beyond 750°C but have not addressed the influences of rafted microstructure on microscopic deformation near the crack tip and FCP behavior. A comprehensive understanding on the effects of rafting under wide-ranging temperatures, correlating with temperature-dependent slip characteristics of γ and γ′ phases, is also required for the engineering application of single-crystal Ni-base superalloys in advanced gas turbines.

The objective of this study is to clarify the effect of rafted microstructures and its temperature dependency on FCP in a single-crystal Ni-base superalloy. Two types of C(T) specimens with rafted microstructures were prepared, and FCP tests were conducted at RT, 450°C, and 700°C. The FCP behaviors of pre-rafted specimens were compared with that of the specimen consisting of the cuboidal γ′ precipitates.[19] The roles of γ′ precipitates in FCP behavior were discussed, by paying a special attention to the microscopic FCP behavior affected by the morphology of γ′ precipitates, the coherency of the γ/γ′ interface, and temperature-dependent slip characteristics of γ and γ′ phases.

2 | EXPERIMENTAL PROCEDURES

The material tested in this study is a single-crystal Ni-base superalloy, CMSX-4. The chemical composition is summarized in Table 1. Heat treatments were conducted as follows: six-stage solution treatment of 1277°C for 2 h, 1288°C for 2 h, 1296°C for 3 h, 1304°C for 3 h, 1313°C for

2 h, 1316°C for 2 h, and 1277°C for 2 h, followed by two-stage aging treatment of 1140°C for 6 h and 871°C for 20 h. After the heat treatment, a regular γ/γ′ microstructure consisting of cuboidal γ′ precipitates embedded in a narrow γ matrix was observed, as shown in Figure 1A.

From the casting ingot with cuboidal γ′ precipitates, a plate-shaped creep specimen was extracted by wire electric discharge machining (EDM) techniques. The geometry of the creep specimen is shown in Figure 2A. Crystal orientations in the loading and specimen's width direction are [001] and [010], respectively. The creep specimen was subjected to a constant tensile stress of 120 MPa at 1080°C for 38 h. This creep loading induced a 0.3% tensile creep strain in the creep specimen. After unloading, the creep specimen was further heat treated at 1080°C for 30 h, which is a subsequent heat treatment to complete a kinetic process of the directional coarsening.[22,23] As a result, a rafted microstructure was completely developed as shown in Figure 1B, which indicates that the directional coarsening occurs in the direction perpendicular to the creep loading axis. From the plate-shaped creep specimen with a rafted microstructure, two types of compact (C(T)) specimens were extracted by EDM techniques, P-type and V-type, as shown in Figure 2B. Here, the crack propagation direction of the P-type specimen is parallel to the coarsening direction, while that of the V-type specimen is perpendicular to the coarsening direction. It should be noted here that the coarsened γ′ precipitate in the V-type specimen is not the so-called "needle-like" shape, but the "plate-like" shape whose normal vector is directed to crack propagation direction in the C(T) specimen. The loading directions of P-type and V-type C(T) specimens are [001] and [010] crystallographic orientations, respectively.

TABLE 1 Chemical composition of CMSX-4 employed in this study (in wt.%)

Co	Cr	W	Al	Ti	Ta	Mo	Re	Ni
9.7	6.5	6.4	5.7	1.0	6.6	0.6	3.0	Bal.

Stress–strain relationships of P-type and V-type specimens at RT are shown in Figure 3, which were measured in tensile tests using miniature tensile specimens extracted from the C(T) specimens. The geometry of a miniature specimen is shown in Figure 2C. It is found in Figure 3 that both P-type and V-type specimens reveal lower yield strength compared with the normal specimen, which consists of the cuboidal γ′ precipitates, although Young's moduli are almost comparable in three types of specimens. It has been also reported by Epishin et al.[27] that the rafted microstructure (similar to the P-type specimen in this study) leads to a lower yield strength at RT and 950°C, although Young's modulus is not affected. A detailed physical basis of the yield strength reduction in the rafted microstructure is still unclear, but it can be related to a misfit relaxation of the coherent γ/γ′ interface induced by the dislocation reaction associated with the rafting phenomenon.

FCP tests were conducted at RT, 450°C, and 700°C using an electro-hydraulic machine coupled with an induction heating system. A constant amplitude sinusoidal wave form was applied under a loading ratio of $R = 0.4$ with a loading frequency of 10 Hz. The stress intensity factor range, ΔK_I, was calculated, conforming to ASTM E647[29]:

$$\Delta K_I = \frac{\Delta P}{BW^{1/2}} F(\xi). \tag{1}$$

$$\text{Here, } \xi = \frac{a}{W}, \tag{2}$$

$$F(\xi) = \frac{2+\xi}{(1-\xi)^{3/2}}\left(0.886 + 4.64\xi - 13.32\xi^2 + 14.72\xi^3 - 5.6\xi^4\right). \tag{3}$$

ΔP, B, W, and a are load range, specimen thickness, width, and projected crack length, respectively. The ΔK_I values at the beginning of FCP tests were 13 to 18 MPam$^{1/2}$, which depends on the microstructure and testing temperature. Before the FCP tests, the specimens

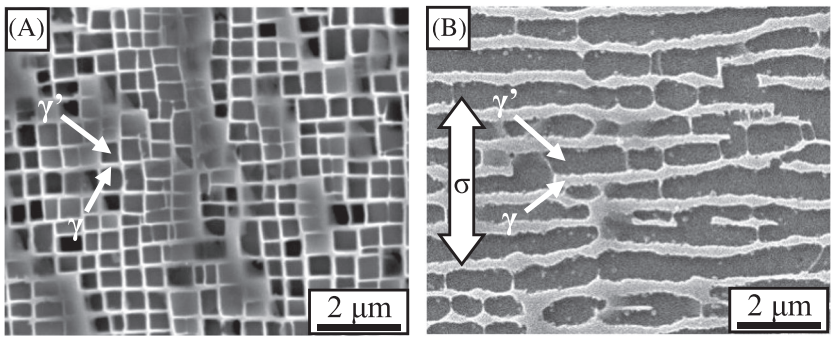

FIGURE 1 Scanning electron microscope (SEM) images of Ni-base superalloy microstructures with (A) cuboidal and (B) plate-like precipitates

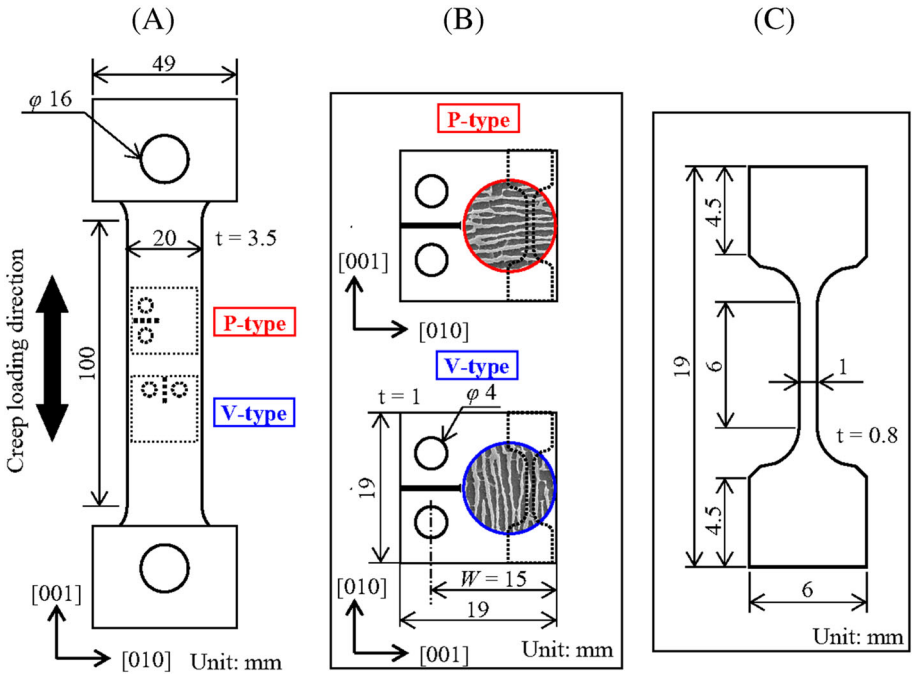

FIGURE 2 Geometries of the (A) creep specimen, (B) C(T) specimen, and (C) miniature tensile specimen

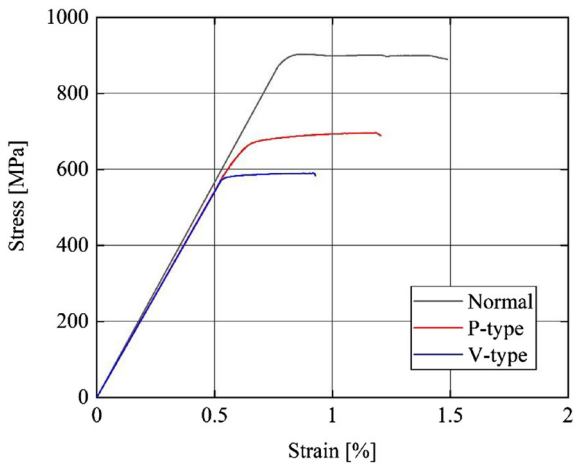

FIGURE 3 Stress–strain relationship of three types of specimen at room temperature

were initially pre-cracked at RT to avoid an influence of initial EDM notch. The load amplitude "ΔP" at the beginning of pre-cracking was 195 N, and the lengths of pre-cracking were about 0.3 mm. The temperature on the specimen surface was monitored and controlled using a type K thermocouple that was connected to a thermometer and induction heating system. Temperature distribution in the gauge section was arranged within ±5°C. Crack lengths on both sides of the C(T) specimens were monitored with digital microscopes. The magnification of the digital microscopes was 1.3 μm/pixel, and an approximate measurement error was less than 5 μm. The average value of the crack lengths on both surfaces was used for the calculations of ΔK_I and FCP rate, da/dN. After the tests, the crack path and fracture surface were observed with a scanning electron microscope (SEM).

3 | EXPERIMENTAL RESULTS

3.1 | Results of FCP tests at RT

Figure 4 shows the FCP test result at RT. The FCP rate is plotted as a function of Mode I stress intensity factor range, ΔK_I, computed based on the projected crack length. Figure 5 shows SEM images of the fracture surface at RT. In Figure 4, red symbols represent the FCP rate of the P-type specimen, while blue symbols represent that of the V-type. These plots are compared with the FCP rate of the normal specimen with the cuboidal γ′ precipitates,[19] which are plotted as black symbols. Triangle symbols mean that the crack propagates in a crystallographic shearing mode along octahedral slip planes, while circle symbols represent the FCP rates when the crack propagates in Mode I opening mode perpendicular to the loading direction. These rules for plotting will be also adopted for the results at 450°C (Figure 8) and 700°C (Figure 11) described later. Some of the data at higher ΔK_I condition in normal and V-type specimens are removed from Figure 4, because they are invalid according to the out-of-plane cracking limits required in ASTM.[29] These invalid data are attributed to the crack plane inclination associated with the crystallographic cracking. The invalid data are not included in the

consideration of this study; however, overall trends are not so different between the valid and invalid data when the FCP rates are evaluated based on ΔK_I. Test results including the invalid FCP rates are shown in the Supporting Information.

As can be seen in Figure 4, there are no significant differences in FCP rates between three types of specimens. However, there is a clear difference in FCP mode as shown in Figure 5. Normal and V-type specimens show the crystallographic shearing mode cracking, which leads to macroscopically inclined crack paths along {111} slip planes as can be seen later in Figure 7. Contrarily, the P-type specimen reveals the opening mode cracking except for the near-surface region. A SEM image of this opening mode fracture surface in the P-type specimen is shown in Figure 6, which is corresponding to the area surrounded by a red square in Figure 5. The fracture surface as seen in Figure 6 is mainly composed of the flat plane (dark gray region) perpendicular to the loading direction but also includes small slip planes (white arrows in Figure 6), which indicates that the shearing mode cracking also takes place microscopically in the P-type specimen.

Figure 7 shows crack paths in three types of specimens observed with SEM. Corresponding positions of Figure 7A–C are indicated as red lines in Figure 5A–C, respectively. For the P-type specimen, the near-surface region was polished to observe the mid-thickness area where the opening mode cracking mainly takes place. It can be seen in Figure 7 that the cracks in normal (Figure 7A) and V-type (Figure 7C) specimens propagate in the crystallographic shearing mode, which penetrates both γ and γ′ phases along {111} octahedral slip planes. On the other hand, the crack in the P-type specimen (Figure 7B) propagates in the γ′ phase and along the γ/γ′ interface, not in the γ phase. In the γ′ phase, the crack

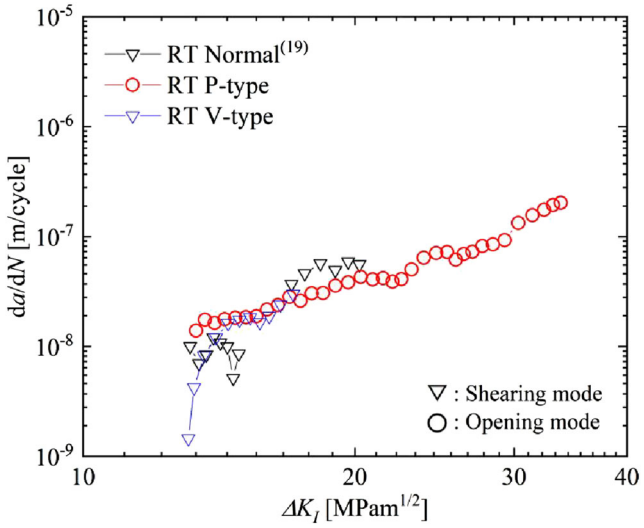

FIGURE 4 Fatigue crack propagation rate at room temperature (RT)

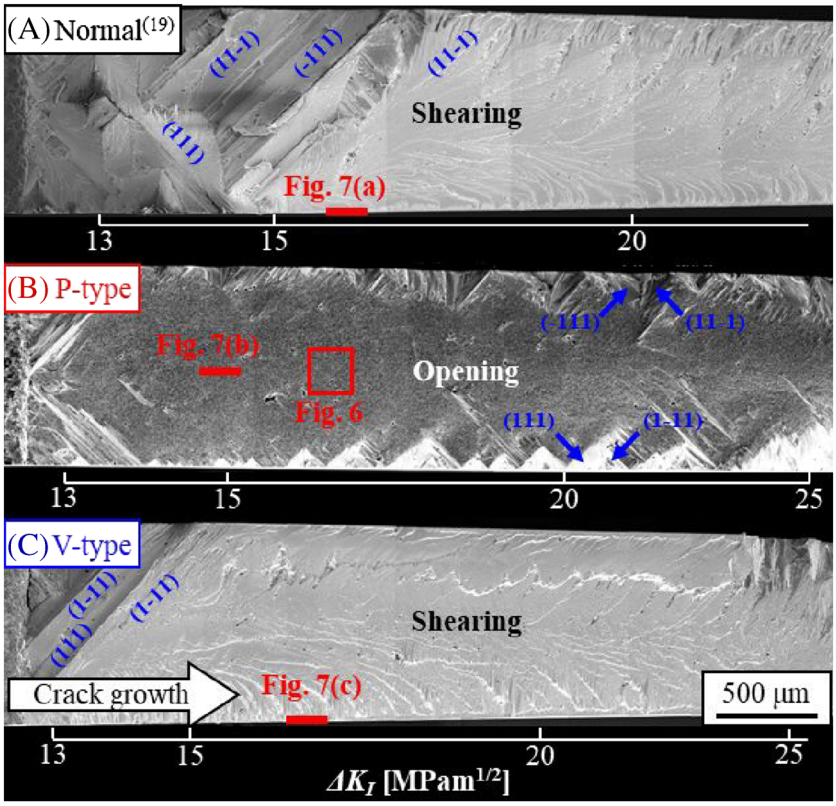

FIGURE 5 Fracture surface at room temperature (RT) after failure

propagates in the shearing mode with a periodic change of the slip planes. According to the SEM images of the fracture surface (Figure 6) and the crack path (Figure 7B), the small fracture surfaces along slip planes in Figure 6 correspond to the crack path within the γ′ phase in Figure 7B, while the opening mode cracking in Figure 6 corresponds to the crack path along the γ/γ′ interface in Figure 7B.

3.2 | Results of FCP tests at 450°C

FCP rates in the three types of specimens at 450°C are shown in Figure 8. The symbols are used in the same way as in Figure 4. In contrast to the result at RT, the FCP rates are strongly affected by the rafted microstructure at 450°C. In low-ΔK condition where all the three specimens showed the opening mode cracking (plotted by circle symbols), the FCP rate of the P-type specimen is slightly higher than that of the normal specimen, while the FCP rate of the V-type specimen is remarkably lower than the other two specimens.

Figure 9 shows the SEM images of fracture surfaces at 450°C. Three specimens reveal a similar cracking mode: The cracks initially propagate in the opening mode and transition to the crystallographic cracking mode when ΔK reaches around 20 MPam$^{1/2}$. Such a transition behavior has been also observed in the study of Suzuki et al.[19] and numerically discussed by Chen and Sakaguchi.[30] These studies have suggested that the ΔK level at the transition is a function of primary (loading direction) and secondary (crack propagation direction) crystal orientations of the C(T) specimen, and it changes between $\Delta K = 14$ and $\Delta K = 23$ MPam$^{1/2}$.[19] It is found in Figure 9 that the transition ΔK is not affected by the rafted microstructure. This means that the transition from the opening mode to shearing mode, which is affected by a geometric relationship between the crack front and octahedral slip planes, is similar even if the morphology of γ′ and coherency of the γ/γ′ interface are changed by the rafting phenomenon. In the V-type specimen, the fracture surface in a lower ΔK regime is unusual where the crack propagates along neither the crystallographic slip planes nor Mode I plane perpendicular to the loading direction. This unusual cracking plane is tilted about 45° with respect to the crack propagation direction, while the crystallographic shearing cracking plane is inclined to "both" the crack propagation and specimen thickness direction. The former cracking plane is categorized as an opening-like mode and plotted by circle symbols in Figure 8, because the corresponding fracture surface shows obviously different features compared with the pure crystallographic shearing cracking. Enlarged fracture surfaces of P-type and V-type specimens are revealed in Figure 9D,E, respectively, which include both the opening (opening-like) and shearing cracking planes.

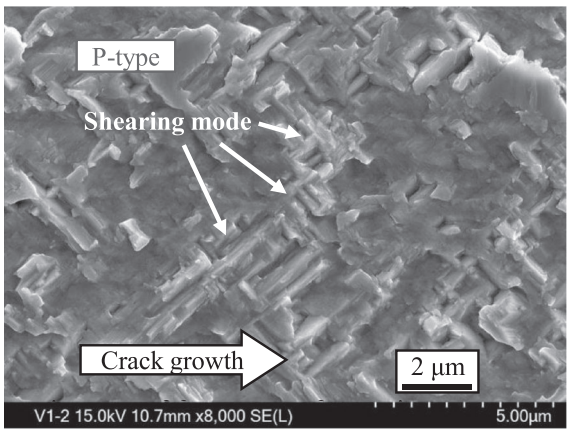

FIGURE 6 Scanning electron microscope (SEM) images of the fracture surface using the P-type specimen at room temperature (RT) (2 mm away from the notch)

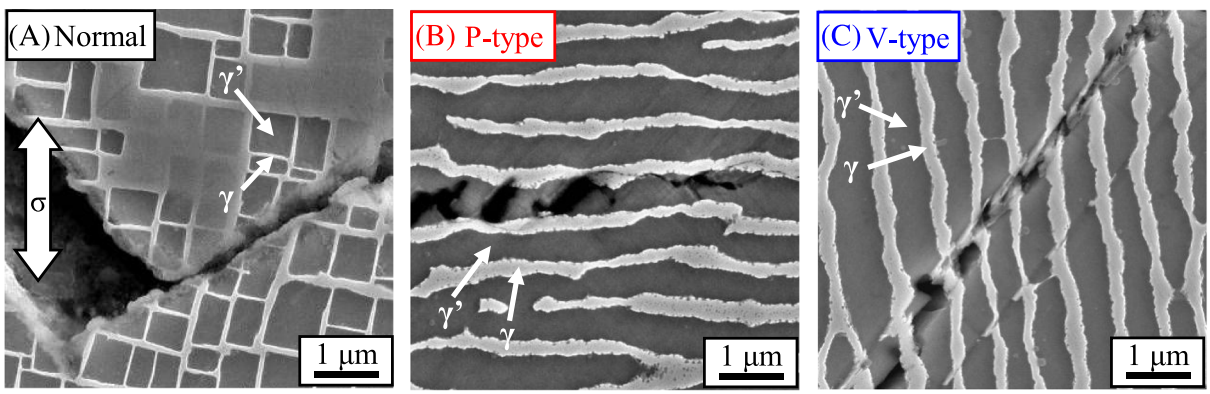

FIGURE 7 Scanning electron microscope (SEM) images of the crack path using (A) normal, (B) P-type, and (C) V-type specimens at room temperature (RT)

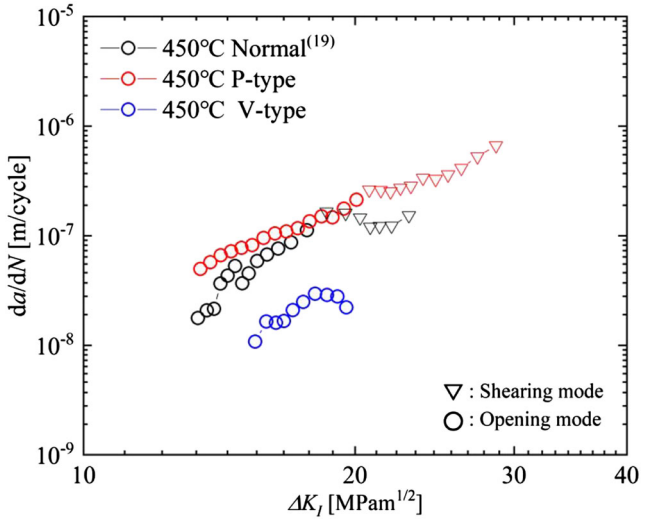

FIGURE 8 Fatigue crack propagation rate at 450°C

Here, the boundaries between the opening (opening-like) and shearing cracking plane are indicated as red arrows, which suggests that the opening-like cracking plane in the V-type specimen is along neither the crystallographic slip planes nor Mode I plane perpendicular to the loading direction.

Figure 10 shows crack paths of the three types of specimens at 450°C. The specimen side surfaces were polished to observe crack paths in the mid-thickness region. Corresponding positions of each crack path are indicated as red lines in Figure 9. It can be seen in Figure 10 that the opening cracks in normal (Figure 10A) and P-type (Figure 10B) specimens propagate within the γ phase. The crack in the normal specimen sometimes hits against the γ′ precipitate and cuts through it in the shearing mode. In the V-type specimen (Figure 10C), the crack propagates in the γ and γ′ phases alternately. A

FIGURE 9 Fracture surface at 450°C after failure

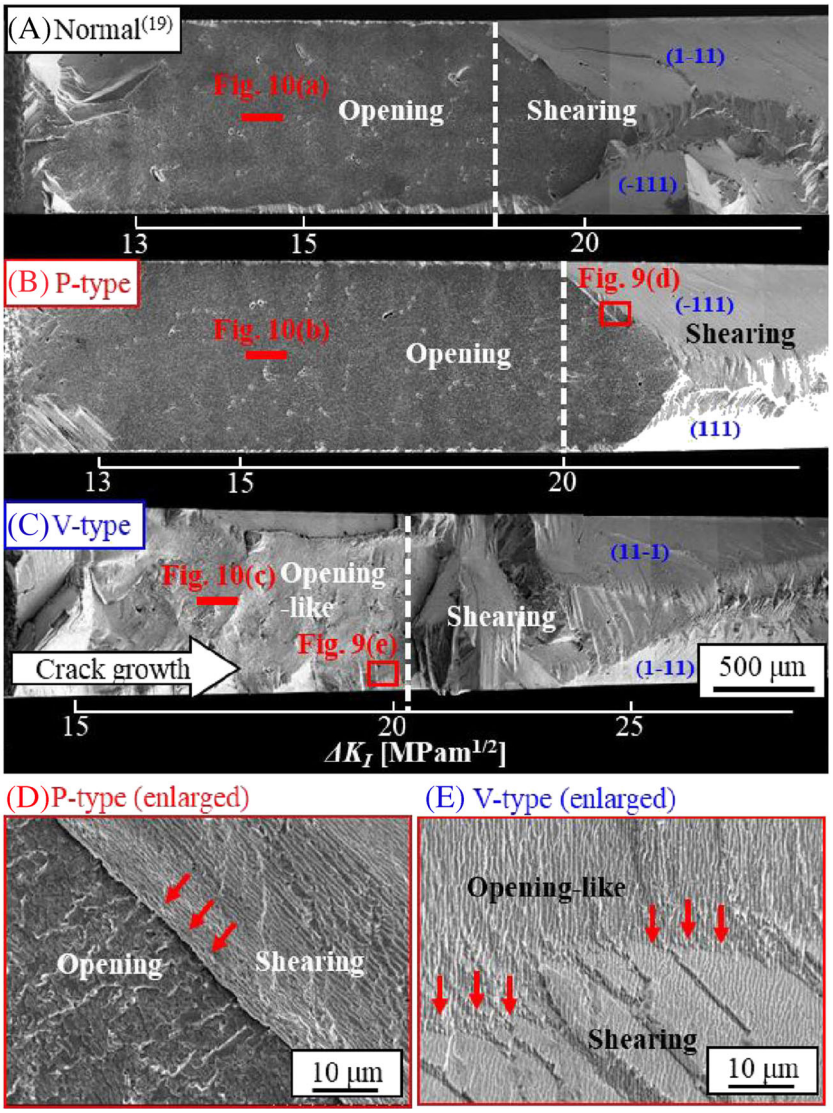

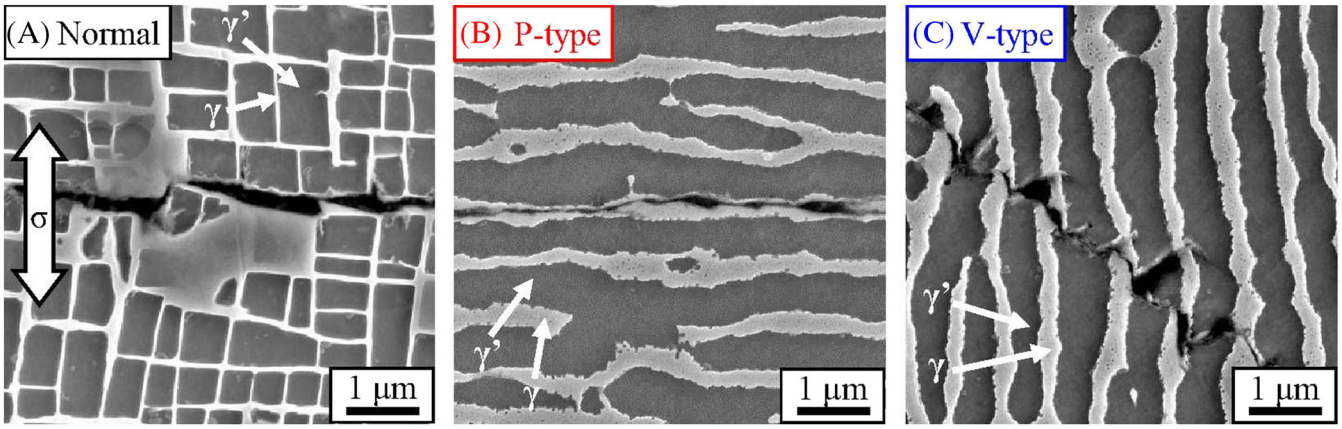

FIGURE 10 Scanning electron microscope (SEM) images of the crack path using (A) normal, (B) P-type, and (C) V-type specimens at 450°C

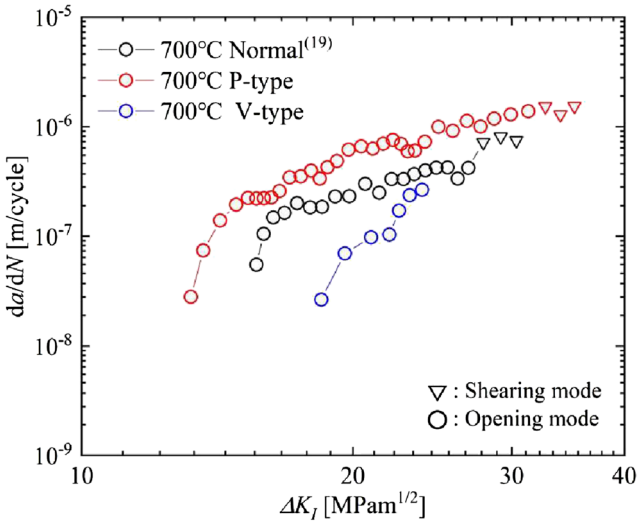

FIGURE 11 Fatigue crack propagation rate at 700°C

resultant macroscopic crack path is tilted with respect to the loading direction, but not along the crystallographic slip plane. Here, the crack propagates in a microscopic zigzag manner and does not show a straight crack path along the slip plane as can be seen in the V-type specimen at RT (Figure 7C). Such a zigzag cracking at 450°C should affect the FCP rate of the V-type specimen, which is remarkably lower than those of normal and P-type specimens. This will be closely discussed in Section 4.2.

3.3 | Results of FCP tests at 700°C

Figure 11 shows FCP rates in three types of specimens at 700°C. The FCP rates show a similar trend to that at 450°C: The FCP rate of the P-type specimen is the highest, followed by normal and V-type specimens. It is found from a comparison between 450°C (Figure 8) and 700°C (Figure 11) that the FCP rates in normal and P-type specimens are higher at 700°C than at 450°C, while the V-type specimen shows comparable FCP rate at 450 and 700°C. Figure 12 shows SEM images of the fracture surface at 700°C. Similar to 450°C, the cracks propagate in the opening mode under a lower ΔK condition and transition to the shearing mode at a certain level of ΔK. Although the microscopic crack path could not be observed clearly in the experiments at 700°C due to oxidation of the crack plane, the phenomenon at 700°C is considered to be similar to that at 450°C. The only difference is found in the ΔK level of transition, which is higher at 700°C than at 450°C: The transition takes place around $\Delta K = 30$ MPam$^{1/2}$ in normal (Figure 12A) and P-type (Figure 12B) specimens, and the V-type specimen (Figure 12C) fails before the transition at 700°C. The transition behavior is a competitive mechanism between the critical resolved shear stress (CRSS) of the γ′ precipitates and resolved shear stress at the crack tip.[19,30] The temperature dependency of the transition behavior is attributed to the temperature-dependent CRSS of γ′ precipitates; that is, a larger shear stress is required to cut through the γ′ precipitates at 700°C, because the CRSS of γ′ precipitates at 700°C is larger than that at 450°C.[19]

4 | DISCUSSIONS

The microscopic mechanism of FCP in ductile solids is essentially dominated by localized deformation along slip bands near the crack tip.[31–33] In the materials with larger grains or single-crystal materials, crack propagation occurs in the direction of the primary slip system, because the crack and the zone of plastic deformation surrounding the crack tip are confined within a few

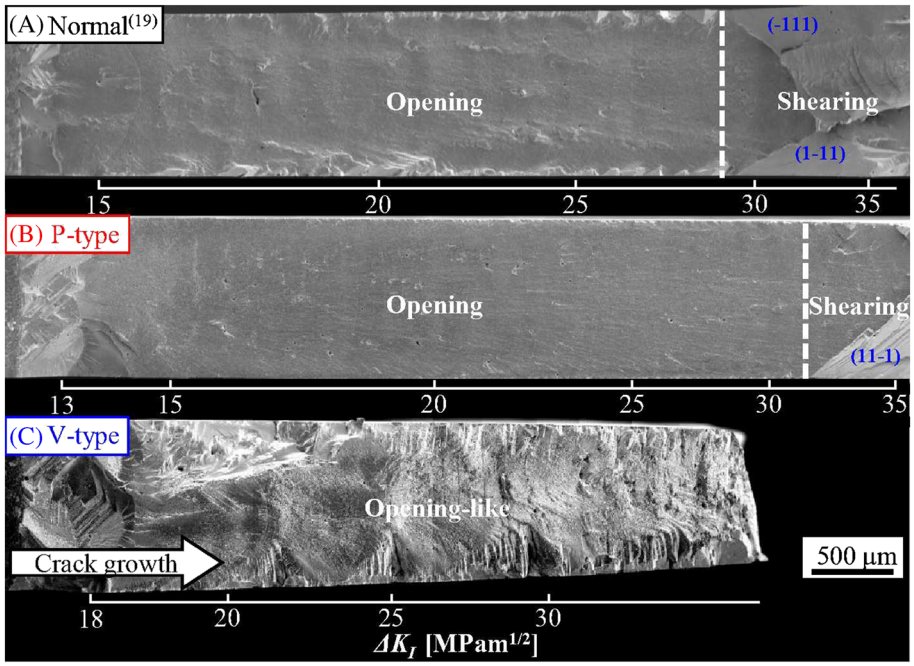

FIGURE 12 Fracture surface at 700°C after failure

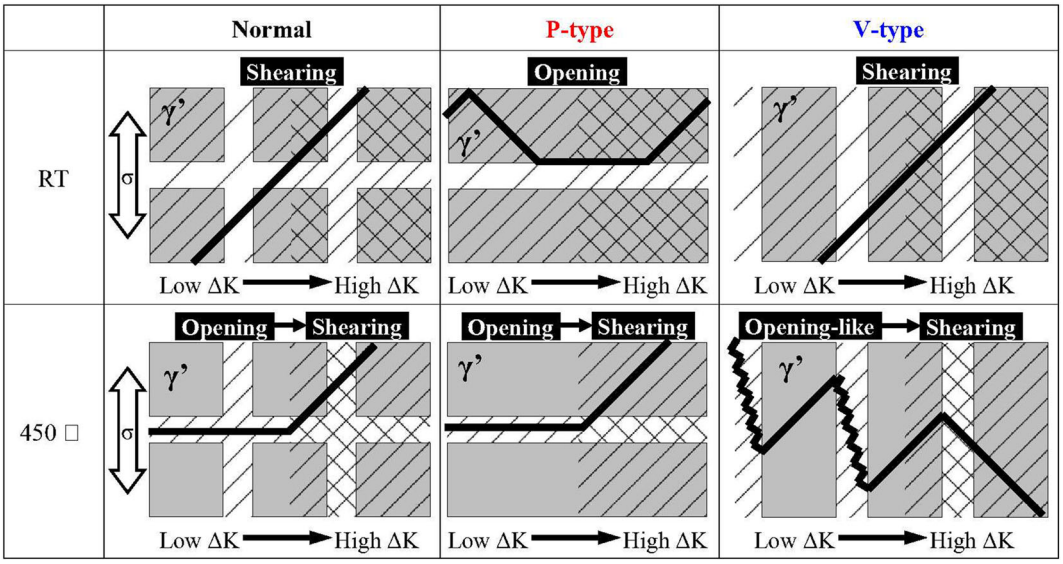

FIGURE 13 Schematic illustrations of the crack path and plastic strain accumulation

grains or a single grain.[34] It has been found that low-temperature FCP in a single-crystal Ni-base superalloy is a function of primary and secondary crystal orientations that alter the geometric relationship between the crack plane and the slip planes and then affect the distribution of localized slip deformation.[30,35] In the case of Ni-base superalloys, the testing temperature is also an important factor that changes the plastic strain distribution near the crack tip associated with the temperature-dependent slip characteristics of γ and γ′ phases. To clarify the effect of a rafted microstructure and its temperature dependency, localized slip deformation near the crack tip should be discussed, considering not only temperature-dependent slip deformation but also microstructural characteristics including the morphology of γ′ precipitates and the coherency between γ and γ′.

Figure 13 schematically summarizes the microscopic crack paths in three types of specimens at RT and 450°C, according to the actual crack paths shown in Figures 7 and 10, respectively. Here, the deformation along octahedral slip planes is schematically drawn as diagonal lines, and the magnitude of slip deformation is represented by line's density. Based on these illustrations, the roles of γ′ precipitates in FCP behavior are discussed in this

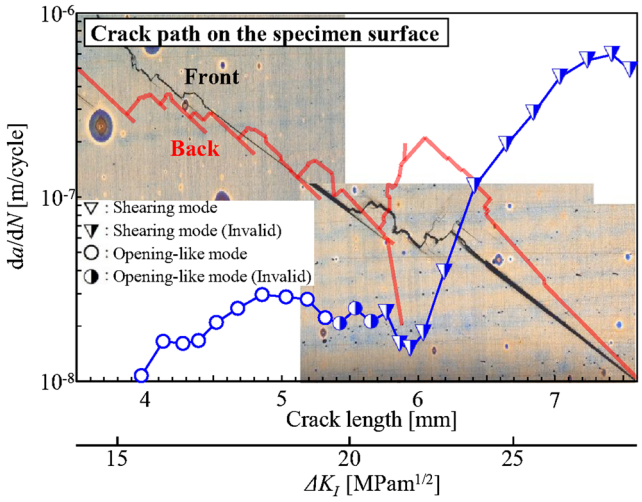

FIGURE 14 Microscope images of the crack path on the specimen surface and FCP rate as a function of crack length at 450°C

chapter, particularly looking at how the microscopic FCP behavior is affected by the morphology of γ′ precipitates, the coherency of the γ/γ′ interface, and temperature-dependent slip characteristics of γ and γ′ phases.

4.1 | FCP behavior at RT

It is found in P-type specimens at RT that the fatigue crack propagates predominantly within the γ′ precipitate, avoiding the γ matrix. This means the resistance to slip deformation and crack propagation is higher in the γ matrix than in the γ′ precipitate at RT. Actually, it has been reported that the CRSS of the γ matrix is higher than that of γ′ precipitates at lower temperature.[4,5] Such a hierarchy between the strength of γ and γ′ is the same in normal and V-type specimens; however, the crack in these two specimens penetrate both γ and γ′. This is due to that the γ′ precipitates, which have lower resistance to crack propagation at RT and are not continuous to the direction of crack propagation in normal and V-type specimens. The higher strength γ matrix is supposed to be a barrier for crack propagation in normal and V-type specimens, but their FCP rates are not much lower than that of the P-type specimen at RT. This is because a difference in slip characteristics between γ and γ′ is not large enough to cause an apparent gap of the FCP rate, even though the γ′ precipitates become a preferential crack path that leads to the pure opening mode cracking in the P-type specimen at RT. Macroscopic yield strength, which is lower in the P-type and V-type specimens as shown in Figure 3, might relate to the microscopic slip deformation and the resultant FCP behavior, but it seems unlikely that the FCP rate at RT is directly correlated with the macroscopic yield strength in this study.

The fatigue crack in the P-type specimen propagates partially along the γ/γ′ interface, as seen in Figure 7B. The FCP along the γ/γ′ interface has also been observed in the rafted microstructure,[25,27,28,36,37] and it has been reported that the rafted γ/γ′ interface tends to increase the FCP rate.[27,37] A loss of γ/γ′ coherency induced by dislocation reaction during the rafting phenomenon might spoil the resistance to the FCP of the γ/γ′ interface. A further investigation is required to seek a role of a coherent γ/γ′ interface in an atomic-scale FCP behavior. A reason for why no cracking occurs along the γ/γ′ interface in the V-type specimen, which has also a rafted microstructure, is that the γ/γ′ interface in the V-type specimen is aligned in the parallel direction to the loading, where the normal stress is not high enough to cause the interface cracking.

4.2 | FCP behavior at higher temperature

As explained in Sections 3.2 and 3.3, the FCP mode at higher temperatures depends on the ΔK level: all the three types of specimens show the transition behavior from the opening or opening-like mode to the crystallographic shearing mode at a certain level of ΔK. The phenomena at 450 and 700°C are almost comparable, but the only difference is found in the ΔK level of transition, which is higher at 700°C than at 450°C. Focusing on the FCP mode at a lower ΔK level before the transition, the fatigue cracks in normal and P-type specimens propagate within the γ matrix at higher temperatures. This suggests that the resistance to slip deformation and crack propagation is lower in the γ matrix at higher temperatures, where the strength hierarchy between γ and γ′ is opposite to that at RT. At a lower ΔK condition in the V-type specimen, the crack propagates in a microscopic zigzag manner and does not show a very straight crack path along the slip plane as seen in this specimen at RT. This should be attributed to the higher CRSS of γ′ at higher temperatures, which prevents large-scale and continuous slip deformation along slip planes.

The FCP rates at higher temperatures, in contrast to the result at RT, are affected by the rafted microstructure, particularly when the cracks propagate in the opening or opening-like mode. According to the crack path as seen in Figure 10, the FCP rate at higher temperatures seems to be influenced by a frequency of hitting against the γ′ precipitates, which has a higher resistance to crack propagation. That is, the fatigue crack in the normal specimen sometimes encounters the γ′ precipitates and has to cut

through them (Figure 10A), while the crack does not have to propagate into the γ′ and can propagate within the softened γ matrix in the P-type specimen (Figure 10B), which shows the highest FCP rate among three specimens. In the V-type specimen, the fatigue crack needs to cross over the strengthened γ′ precipitates each time (Figure 10C). This is one of the reasons for the significantly lower FCP rate of the V-type specimen in a lower ΔK condition under higher temperatures. The difference in the FCP rate between P-type and normal specimens becomes larger when the testing temperature increases from 450 to 700°C as can be seen in Figures 8 and 11. This is attributed to the fact that the increase in temperature (1) leads to the reduction of the crack propagation resistance in the γ matrix, which is a preferential crack path at both 450 to 700°C, and (2) also leads to the increase of the crack propagation resistance in the γ′ precipitate, which plays the barrier role for crack propagation in the normal specimen.

The lower FCP rate of the V-type specimen is also associated with the unusual cracking mode as can be seen in the fracture surfaces (Figures 9C and 12C) and crack path (Figure 10C), where the crack propagates along neither the crystallographic slip planes nor the Mode I plane perpendicular to the loading direction. Figure 14 replots the FCP rate of the V-type specimen at 450°C as a function of the crack length, where the observed crack path on the specimen's side surface is also indicated in the same scale. The invalid data, which violate the out-of-plane cracking limits, are also plotted in Figure 14 for comparison. These invalid FCP rates are plotted in half-solid symbols to distinguish them from the valid data. It is found that the FCP rate under the condition of $\Delta K < 21\ \mathrm{MPam}^{1/2}$ does not increase with crack length, which might be associated with frequent crack deflection and branching.[25] Then, the FCP rate drastically increases when ΔK exceeds $23\ \mathrm{MPam}^{1/2}$, where the crack propagates in a very straight manner. The crack deflection and branching at a lower ΔK condition should be attributed to the higher CRSS of γ′ at higher temperatures and the zigzag crack propagation in the mid-thickness region as seen in Figure 10C, which prevent the straightforward slip deformation and crack propagation along a single slip plane. A combined-mode cracking, which includes the crystallographic cracking near the surface and the opening-like mode zigzag cracking in the mid-thickness region, would lead to a significant reduction of the FCP rate. This is the other reason for the lower FCP rate under a lower ΔK condition in the V-type specimen, compared with the pure opening mode cracking in normal and P-type specimens and also compared with the pure shearing mode cracking under a higher ΔK condition in the V-type specimen.

In summary, the effect of a rafted microstructure on the FCP rate is only remarkable under a lower ΔK condition under higher temperatures, where the fatigue cracks propagate in the opening or opening-like mode. In other words, the FCP rates in the crystallographic shearing mode, which takes place in higher ΔK and lower temperature, are not so affected by the rafted microstructure.

5 | CONCLUSIONS

The effects of a rafted microstructure and its temperature dependency on FCP in a single-crystal Ni-base superalloy are investigated experimentally. FCP tests are conducted at RT, 450°C, and 700°C using two types of C(T) specimens with a rafted microstructure and P-type and V-type specimens. The coarsening direction of the rafted microstructure in the P-type specimen is parallel to the crack propagation direction, while that in the V-type specimen is perpendicular to the propagation direction. The results of FCP tests for P-type and V-type specimens are compared with those of the normal specimen with the cuboidal γ′ precipitates. The conclusions derived from the investigations are summarized as follows:

i. At RT, there is no significant difference in FCP rates between the three types of specimens. However, there is a clear difference in the FCP mode. Normal and V-type specimens show a crystallographic shearing mode cracking that penetrates both γ and γ′ phases, while the P-type specimen reveals an opening mode cracking that propagates within the γ′ phase and along the γ/γ′ interface.
ii. At 450 and 700°C, the FCP in all three types of specimens reveals a similar cracking mode: The cracks initially propagate in the opening mode and transition to the crystallographic cracking mode at a certain level of ΔK. The FCP rates are affected by the rafted microstructure under a lower ΔK condition, where the cracks propagate in the opening mode or opening-like mode. The FCP rate of the P-type specimen is slightly higher than that of the normal specimen, while the FCP rate of the V-type specimen is remarkably lower than that of the other two specimens. The FCP rates in the crystallographic shearing mode, which takes place in higher ΔK and lower temperature, are not so affected by the rafted microstructure.

ACKNOWLEDGMENT

We would like to thank Mr. Yusuke Sakurai for his contribution to the setup of the fatigue crack propagation tests.

DATA AVAILABILITY STATEMENT

The data that support the findings of this study are available from the corresponding author upon reasonable request.

ORCID

Motoki Sakaguchi https://orcid.org/0000-0003-2862-4731

REFERENCES

1. Reed RC. *The Superalloys: Fundamentals and Applications*. UK: Cambridge University Press; 2006.
2. Sengupta A, Putatunda SK. Kinetics of γ' precipitation and its influence on fatigue crack growth behavior of a new single-crystal nickel-based superalloy (CMSX-4G) at room temperature. *J Mater Eng Perform*. 1993;2(1):57-68.
3. Sengupta A, Putatunda SK, Balogh M. Fatigue crack growth behavior of a new single crystal nickel-based superalloy (CMSX-4) at 650 °C. *J Mater Eng Perform*. 1994;4(4):540-550.
4. Pope DP, Ezz SS. Mechanical properties of Ni3AI and nickel-base alloys with high volume fraction of γ′. *Int Met Rev*. 1984; 29:136-167.
5. Lall C, Chin S, Pope DP. The orientation and temperature dependence of the yield stress of Ni3 (AI, Nb) single crystals. *Metall Trans A*. 1979;10A:1323-1332.
6. Leverant GR, Gell M. The influence of temperature and frequency on the fatigue fracture of cube oriented nickel-base superalloy single crystals. *Metall Trans A*. 1975;6A(2):367-371.
7. Lerch BA, Antolovich SD. Fatigue crack propagation behavior of a single crystalline superalloy. *Metall Trans A*. 1990;21A: 2169-2117.
8. Lupinc V, Onofrio G, Vimercati G. The effect of creep, oxidation and crystal orientation on high temperature fatigue crack propagation in standard and raft-like gamma prime CMSX-2. In: *Superalloys 1992*. Warrendale PA: TMS; 1992:717-726.
9. Henderson MB, Martin JW. The influence of crystal orientation on the high temperature fatigue crack growth of a Ni-based single crystal superalloy. *Acta Mater*. 1996;44(1):111-126.
10. Telesman J, Ghosn LJ. Fatigue crack growth behavior of PWA 1484 single crystal superalloy at elevated temperatures. *J Eng Gas Turbines Power*. 1996;118(2):399-405.
11. Kakehi K. Influence of primary and secondary crystallographic orientations on strengths of nickel-based superalloy single crystals. *Mater Trans*. 2004;45(6):1824-1828.
12. Sakaguchi M, Tsuru T, Okazaki M. Fatigue crack propagation in thin-wall superalloys component; experimental investigation via miniature CT specimen. In: *Superalloys 2012*. Warrendale PA: TMS; 2012:431-437.
13. Adair BS, Johnson WS, Antolovich SD, Staroselsky A. Crystallographic orientation and temperature effects on the fatigue crack growth rate and resulting fracture surface morphology in PWA1484 single crystal superalloy. *Fatigue Fract Eng Mater Struct*. 2015;38(1):56-68.
14. Sakaguchi M, Komamura R, Hosaka Y, Inoue H. Stage I fatigue crack propagation in a single crystal and a directional solidified Ni-base superalloy. In: *Superalloys 2016*. Warrendale PA: TMS; 2016:639-646.
15. Busse C, Palmert F, Sjodin B, et al. Evaluation of the crystallographic fatigue crack growth rate in a single-crystal nickel-base superalloy. *Int J Fatigue*. 2019;127:259-267.
16. Ormastroni LMB, Suave LM, Cervellon A, Villechaise P, Cormier J. LCF, HCF and VHCF life sensitivity to solution heat treatment of a third-generation Ni-based single crystal superalloy. *Int J Fatigue*. 2020;130:105247.
17. Li P, Jiang W, Rui SS, et al. Effect of misorientation on the fatigue life of nickel-base single crystal superalloy DD5 at 980 °C. *Int J Fatigue*. 2021;153:106479.
18. Telesman J, Ghosn LJ. The unusual near-threshold FCG behavior of a single crystal superalloy and the resolved shear stress as the crack driving force. *Eng Fract Mech*. 1989;34(5-6): 1183-1196.
19. Suzuki S, Sakaguchi M, Inoue H. Temperature dependent fatigue crack propagation in a single crystal Ni-base superalloy affected by primary and secondary orientations. *Mater Sci Eng A*. 2018;724:559-565.
20. Nabarro FRN. Rafting in superalloys. *Metall Mater Trans, A*. 1996;27A:513-530.
21. Pollock TM, Argon AS. Directional coarsening in nickel-base single crystals with high volume fractions of coherent precipitates. *Acta Matell Mater*. 1994;42(6):1859-1874.
22. Sakaguchi M, Ike M, Okazaki M. Microstructural changes in a single crystal Ni-base superalloy induced by plastic straining. *Mater Sci Eng A*. 2012;534:253-259.
23. Sakaguchi M, Okazaki M. Distinctive role of plastic and creep strain in directional coarsening of a Ni-base single crystal superalloy. *Mater Sci Eng A*. 2018;710:121-128.
24. Socrate S, Parks DM. Numerical determination of the elastic driving force for directional coarsening in Ni-superalloys. *Acta Matell Mater*. 1993;42:2185-2209.
25. Ott M, Mughrabi H. Dependence of the high temperature low-cycle fatigue behavior of the monocrystalline nickel-base superalloys CMSX-4 and CMSX-6 on the γ/γ′-morphology. *Mater Sci Eng A*. 1999;272(1):24-30.
26. Sakaguchi M, Okazaki M. Fatigue life evaluation of a single crystal Ni-base superalloy, accompanying with change of microstructural morphology. *Int J Fatigue*. 2007;29(9-11):1959-1965.
27. Epishin A, Link T, Nazmy M, Staubli M, Klingelhoffer H, Nozle G. Microstructural degradation of CMSX-4: kinetics and effect on mechanical properties. In: *Superalloys 2008*. Warrendale PA: TMS; 2008:725-731.
28. Yang XG, Tan L, Sui TX, Shi DQ, Fan YS. Low cycle fatigue behaviour of a single crystal Ni-based superalloy with a central hole: effect of inhomogeneous rafting microstructure. *Int J Fatigue*. 2021;153:106467.
29. Standard test method for measurement of fatigue crack growth rates, annual book of ASTM standards E647-08. *ASTM Int*. 2010;669-713.
30. Chen X, Sakaguchi M. Transition behavior from mode I cracking to crystallographic cracking in a Ni-base single crystal superalloy. *Int J Fatigue*. 2020;132:105400.
31. Pineau A, McDowell DL, Busso EP, Antolovich SD. Failure of metals II: fatigue. *Acta Mater*. 2016;107:484-507.
32. Guan Y, Chen B, Zou J, Britton BT, Jiang J, Dunne FP. Crystal plasticity modelling and HR-DIC measurement of slip activation and strain localization in single and oligo-crystal Ni alloys under fatigue. *Int J Plast*. 2017;88:70-88.

33. Lu X, Dunne FP, Xu Y. A crystal plasticity investigation of slip system interaction, GND density and stored energy in non-proportional fatigue in nickel-based superalloy. *Int J Fatigue*. 2020;139:105782.
34. Suresh S. *Fatigue of Materials*. UK: Cambridge University Press; 1991.
35. Sakaguchi M, Komamura R, Chen X, Higaki M, Inoue H. Crystal plasticity assessment of crystallographic stage I crack propagation in a Ni-based single crystal superalloy. *Int J Fatigue*. 2019;123:10-21.
36. Henderson MB, Martin JW. Influence of precipitate morphology on the high temperature fatigue properties of SRR99. *Acta Matell Mater*. 1995;43(11):4035-4043.
37. Cervellon A, Cormier J, Mauget F, Hervier Z. VHCF life evolution after microstructure degradation of a Ni-based single crystal superalloy. *Int J Fatigue*. 2017;104:251-262.

SUPPORTING INFORMATION

Additional supporting information can be found online in the Supporting Information section at the end of this article.

How to cite this article: Sakaguchi M, Okamoto R, Karato T, Suzuki K. Effect of rafted microstructure and its temperature dependency on fatigue crack propagation in a single-crystal Ni-base superalloy. *Fatigue Fract Eng Mater Struct*. 2022;1-13. doi:10.1111/ffe.13888